https://doi.org/10.3311/PPee.36813

Periodica Polytechnica Electrical Engineering and Computer Science

Metamodel-based Optimization of Anisotropic Rotor Axial Flux Permanent Magnet Synchronous Motors

Attila Nyitrai[1*], Miklós Kuczmann[1]

[1] Department of Power Electronics and Electric Drives, Széchenyi István University, Egyetem tér 1., H-9026 Győr, Hungary
[*] Corresponding author, e-mail: nyitrai.attila@sze.hu

Received: 05 March 2024, Accepted: 18 December 2024, Published online: 14 January 2025

Abstract

Axial flux motors have some significant advantages over radial flux motors in high torque-density applications. However, the optimization of axial flux permanent magnet synchronous motors is a challenging task; the analysis usually requires 3D finite element analysis or the application of the 2D multi-slice method. In this paper a novel single-surrogate multi-slice method (SS-MSM) is proposed for modeling anisotropic rotor axial flux permanent magnet motors. However, the general methodology can be applied to other axial flux motors as well. A model calibration methodology has been described where the SS-MSM parameters have been determined using a 2D finite element approach as a reference. The SS-MSM was found to be suitable for a fast and reasonably accurate approximation of the motor performance. Based on the described analysis method, an efficient optimization approach is proposed.

Keywords

axial flux motors, metamodel-based optimization, single-surrogate multi-slice method

1 Introduction

This paper summarizes the research on the metamodel-based optimization method of anisotropic rotor axial flux permanent magnet synchronous motors (AnR-AFPMSM). Machine learning (deep learning) based methods have been in the focus of research on e-motor optimization recently. However, the method is mostly applied on radial flux motors, or in case of axial flux motors, mostly on simple 2D equivalents or complete 3D models. The method proposed here has the novelty of training the surrogate model on a general parametric 2D model (slice) and assemble the multi-slice equivalent from separate parameterized surrogate results. These results can be used directly through optimization, or a second layer of surrogate model can be built and used for optimization. The optimization methods described in the literature are mostly developed for axial flux surface-mounted permanent magnet motors (AF-SPMSM) [1, 2]. However, as presented in [3], the axial flux permanent magnet motors with anisotropic rotor designs have a more complex geometry according to Fig. 1–3 and a larger number of parameters. In addition, in the case of the AnR-AFPMSM, due to the magnetic anisotropy of the motor, the d- and q-axis inductances are different and not constant [4]. The optimal current angle, assuming MTPA control strategy, may change during geometry optimization and is also a function of the stator

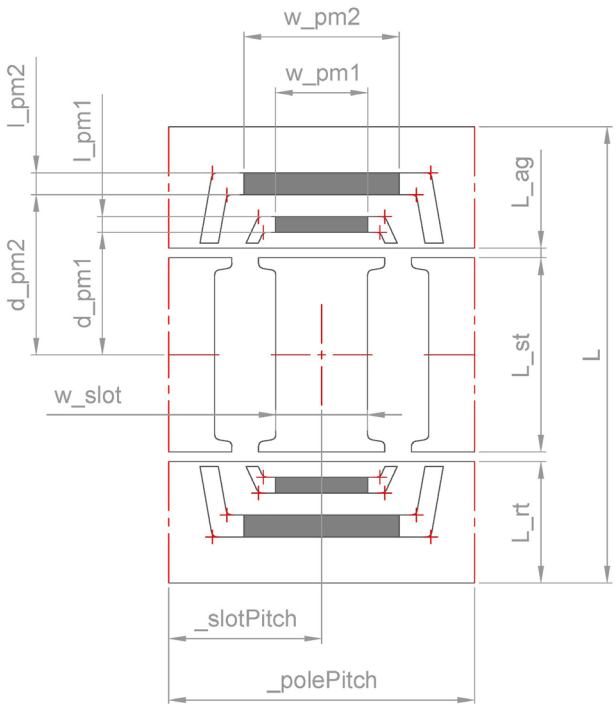

Fig. 1 Main geometrical parameters of the AnR-AFPMSM

Cite this article as: Nyitrai, A., Kuczmann, M. "Metamodel-based Optimization of Anisotropic Rotor Axial Flux Permanent Magnet Synchronous Motors", Periodica Polytechnica Electrical Engineering and Computer Science, 2025. https://doi.org/10.3311/PPee.36813

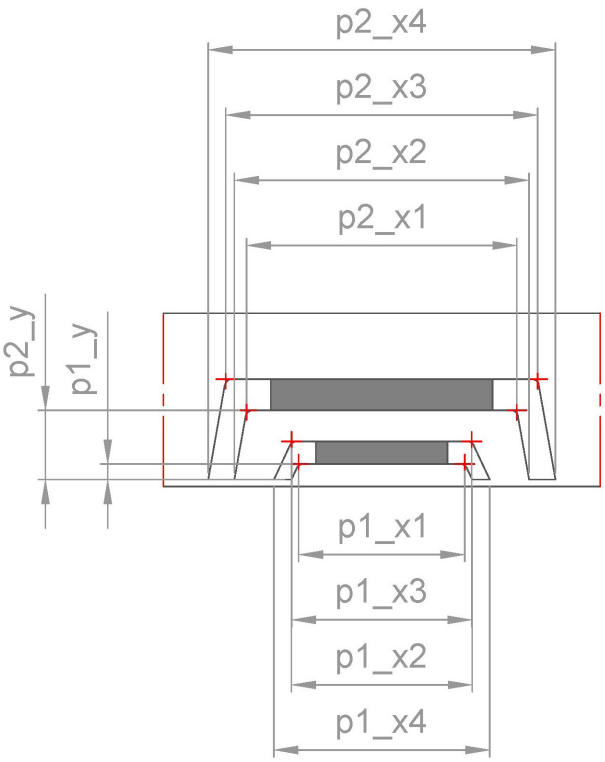

Fig. 2 Flux barrier geometrical parameters of the AnR-AFPMSM

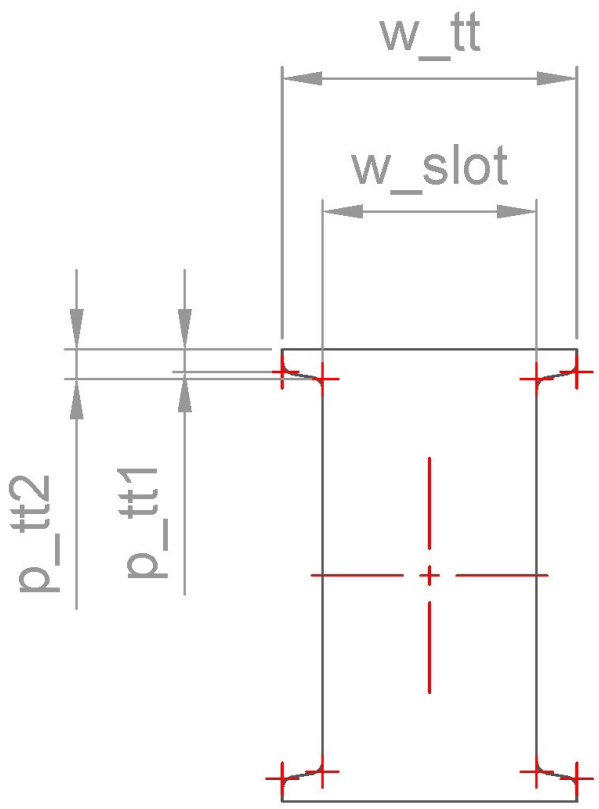

Fig. 3 Stator segment geometrical parameters of the AnR-AFPMSM

current due to saturation effects. Therefore, the optimization procedure of AnR-AFPMSMs is more complex than the simple AFPMSMs and would require large computational resources if direct optimization approaches using 3D [5] or 2D multi-slice methods [6] were used.

Therefore, the AnR-AFPMSM optimization problem incorporates all the difficulties of both radial flux IPM and axial flux motor designs. To efficiently optimize this type of motor, a metamodel-based approach, the single-surrogate multi-slice method (SS-MSM), has been proposed. This approach ensures that the optimizer can compute an appropriate number of design points in a reasonable time, given the otherwise computationally expensive simulation and the relatively large number of input parameters.

1.1 Design description

The reference design is described in [3]. In general, axial flux electric motors have advantages over radial flux topologies such as higher torque density, modular design, and a higher diameter to length ratio, which can be an advantageous in some cases for drive system packaging [7].

Electric traction applications require a wide operating speed range for a given DC link voltage available to the inverter from the vehicle battery [8]. Therefore, surface permanent magnet motors (SPM) have the major disadvantage of having a magnetically non-salient (isotropic) rotor structure, where there is only a negligible reluctance effect. The field-weakening capability of SPMs is limited. On the other hand, the electromagnetic torque of anisotropic (salient) structures consists of two components: the alignment (PM) torque and the reluctance torque. By changing the current angle, it is possible to operate these kinds of motors above the base speed, in the field-weakening region. In this operating range, the magnet flux is weakened, so a high-speed operating point does not violate the voltage limit. However, a suitable winding is required to achieve different quadrature- and direct-axis inductances: an axial flux motor topology with anisotropic rotor geometry and fractional slot distributed winding has been proposed in [3].

In this study, the proposed method is presented through a simplified example. The basic design parameters are given in Table 1. The motor has a dual-rotor (single stator) arrangement. It has 24 slots (or stator segments) and 10 poles, while using a fractional-slot distributed winding. The rotor has 2 magnet layers.

Table 1 Motor topology and basic parameters

Motor type	AnR-AFPMSM
Motor arrangement	Dual rotor
Number of slots	24
Number of poles	10
Winding type	FSDW
Winding layers	2
Winding configuration	AA|bb|aC|Ba|cc| AA|Cb|aC|BB|cc| bA|Cb|…
Magnet layers	2

1.2 Geometric parameters

The geometric parameters of the AnR-AFPMSM can be represented in the real 3D form or by the 2D slices. Therefore, the 2D representation has a different geometry for each slice. The main 2D geometrical parameters are shown in Fig. 1, such as the stator and rotor lengths, the air-gap length and the dimensions and positions of the permanent magnets. The detailed rotor geometry and stator segment dimensions are shown in Figs. 2 and 3. The absolute values of the geometry parameters of the reference design are defined in Table 2. During the metamodeling phase and optimization, the parametrization was used indirectly through a ratio-based approach as described in Section 3.1.

2 Modeling of the AnR-AFPMSM

The electromagnetic modeling of axial flux motors is a geometrically three-dimensional problem. However, several methods exist to reduce the problem to two dimensions [9–13]. A detailed description of the AnR-AFPMSM and its modeling methods is given in [3]. An analytical magnetic equivalent circuit model and a finite element model of the motor with anisotropic rotor design were also presented. In the present study, the 2D multi-slice method based on finite element analysis was applied to generate the training dataset for the metamodeling. Applying this method, the 3D geometry of the motor was represented by a number (n) of 2D models (Fig. 4). The 2D part-models (slices) together are the 2D equivalent model which needs to be evaluated in case of all the design points. The actual parameters of the slices can be calculated by the following equation [3]:

$$P_n\left(r_i\right) = P\left(r_{mean}\right) \cdot \frac{r_i}{r_{mean}}.$$

The number of slices was selected to be 5 during the analysis of the example geometry. The FEA model was built in ANSYS Maxwell.

Table 2 Absolute geometric parameters of the AnR-AFPMSM reference design

ID	Reference value	Description
D_{So}	400 mm	Stator outer diameter
D_{Si}	260 mm	Stator inner diameter
l_S	59 mm	Stator active length
l_R	67.5 mm	Rotor active length
l_g	1.1 mm	Airgap length
w_{pm1}	29.5 mm	Magnet width, layer 1
w_{pm2}	50.6 mm	Magnet width, layer 2
l_{pm1}	4.9 mm	Magnet length, layer 1
l_{pm2}	10.8 mm	Magnet length, layer 2
d_{pm1}	42.1 mm	Magnet position, layer 1
d_{pm2}	68.7 mm	Magnet position, layer 2
w_S	16.2 mm	Slot width
τ_S	43.2 mm	Slot pitch
τ_P	103.7 mm	Pole pitch
p_{1x1}	31.4 mm	Flux barrier, layer 1 (Fig. 2)
p_{1x2}	38.5 mm	Flux barrier, layer 1 (Fig. 2)
p_{1x3}	33.5 mm	Flux barrier, layer 1 (Fig. 2)
p_{1x4}	40.6 mm	Flux barrier, layer 1 (Fig. 2)
p_{2x1}	59.1 mm	Flux barrier, layer 1 (Fig. 2)
p_{2x2}	72.4 mm	Flux barrier, layer 1 (Fig. 2)
p_{2x3}	70.3 mm	Flux barrier, layer 1 (Fig. 2)
p_{2x4}	84.6 mm	Flux barrier, layer 1 (Fig. 2)
p_{1y}	1.8 mm	Flux barrier (Fig. 2)
p_{2y}	22.4 mm	Flux barrier (Fig. 2)

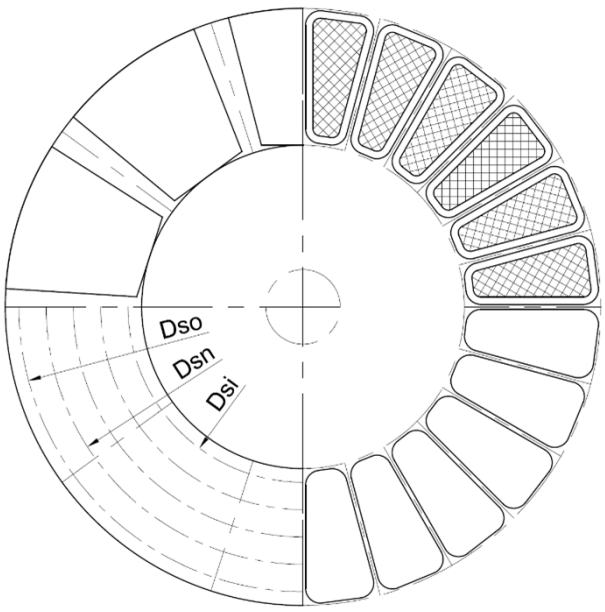

Fig. 4 Multi-slice decomposition of the 3D axial flux motor geometry

2.1 Metamodeling approaches

The basic idea of metamodeling is to create a mathematical model (metamodel or surrogate model), that can be quickly evaluated on the design space and can approximate the responses (output parameters) with reasonable accuracy. Using the metamodel, an optimization algorithm can work more efficiently, allowing a greater number of iterations on a smoother response surface. Recently, several researchers have focused on metamodel-based approaches in electric motor design. An optimization method for cogging torque minimization of axial flux motors is proposed in [14]. Multi-objective, metamodel-based optimization approaches of different motor types are described in [15–17] and a metamodel-based robust design approach is presented in [18]. Some of the main advantages of using metamodeling in electric motor design are reduction of complexity (parameter reduction), evaluation of parameter sensitivity, computationally less expensive re-evaluation of the metamodel than the original (FEM) model and better understanding of the design (evaluation of parameter importance).

However, it is necessary to evaluate the approximation quality of the surrogate models to decide whether the model is suitable for further analysis, such as parametric variational analysis or optimization, based on its approximations. In general, the complexity of the surrogate model depends on the complexity of the physical phenomena to be approximated and the parameter ranges (design space) that need to be covered. Obviously, even a complex physical problem can have an almost linear behavior in a small design space. Therefore, it is not obvious which mathematical model and parametrization to choose to obtain a reasonably accurate surrogate model and an overall efficient process. To automatically select the best metamodel for a given problem, an objective metamodel quality measure was proposed in [19].

An important feature of metamodeling is the ability to reduce the number of input parameters. To determine which input parameters are significant, linear, or quadratic correlation coefficients can be calculated:

$$\rho_{ij} = \frac{1}{N-1} \frac{\sum_{k=1}^{N} \left(y^{(k)} x_i - \mu_y \left(x_i \right) \right) \left(x_j^{(k)} - \mu_{x_j} \right)}{\sigma_{y(x_i)} \sigma_{x_j}}. \tag{1}$$

It is assumed that a correlation coefficient $\rho_{ij} < 0.3$ indicates a weak correlation between parameters i and j. A correlation coefficient $\rho_{ij} < 0.7$ indicates a strong correlation. The correlation coefficients can be summarized in a correlation matrix. The significance of the input parameters is determined based on the calculated correlations, and the insignificant parameters can be filtered out. In general, the sum of squares is used as a statistical measure of variability. The total variability consists of two parts: the variability explained by the regression model and the variability that cannot be explained. For example, in the case of a simple polynomial regression, to evaluate the approximation quality, the coefficient of determination (CoD) metric introduced in [20] can be used to evaluate the quality of the approximation:

$$R^2 = \frac{SS_R}{SS_T} = 1 - \frac{SS_E}{SS_T}, \tag{2}$$

where $SS_T = \sum_{i=1}^{N} \left(y_i - \mu_Y \right)^2$ is the total variation (sum of squares total), $SS_R = \sum_{i=1}^{N} \left(\hat{y}_i - \mu_{\hat{Y}} \right)^2$ is the explained variation (sum of squares due to regression) and $SS_E = \sum_{i=1}^{N} \left(y_i - \hat{y}_i \right)^2$ is the unexplained variation (sum of squared errors). Therefore:

$$\sum_{i=1}^{N} \left(y_i - \mu_Y \right)^2 = \sum_{i=1}^{N} \left(\hat{y}_i - \mu_{\hat{Y}} \right)^2 + \sum_{i=1}^{N} \left(y_i - \hat{y}_i \right)^2. \tag{3}$$

To penalize overfitting that can occur when using an increased amount of model coefficients p compared to the number of data points N, the adjusted CoD was introduced in [20]:

$$R_{adj}^2 = 1 - \frac{N-1}{N-p} \left(1 - R^2 \right). \tag{4}$$

After the significance filtering of the input parameters, the importance of the remaining input parameters can be determined by calculating the difference between the coefficient of determination of the full and the reduced model. The coefficient of importance was in introduced in [21]:

$$\begin{aligned} \mathrm{CoI}_{X_i,Y} &= \mathrm{CoD}_Y \left(X_1, \ \ldots, \ X_n \right) \\ &- \mathrm{CoD}_Y \left(X_1, \ \ldots, \ X_{i-1}, \ X_{i+1}, \ \ldots, \ X_n \right). \end{aligned} \tag{5}$$

The coefficient of prognosis (CoP) is a model-independent metric introduced by Most and Will in [19] and calculated on the test data set:

$$\mathrm{CoP} = 1 - \frac{SS_E^{Pred}}{SS_T}. \tag{6}$$

This approach is an error estimation using a cross-validation method. The dataset is divided into k subsets. The metamodel is trained on each combination of $k - 1$ subsets. The remaining subset in each iteration (validation set) is used to calculate the model prediction error (SS_E^{Pred}). In the automatic process, the metamodel CoP is calculated for each metamodel generated. The model with the highest CoP value is selected and called the metamodel of optimal prognosis (MOP).

2.2 Single-Surrogate Multi-Slice Method

In this study, a single-surrogate multi-slice method is proposed. The flowchart of the method is shown in Fig. 5. The method is based on a 2D multi-slice decomposition of the 3D geometry of the AnR-AFPMSM. In general, the multi-slice method alone can be applied to both analytical and numerical (FEM) models. In the proposed method, the multi-slice decomposition method is used in combination with a parametric finite element model, controlled by an algorithm to generate a surrogate model. The methodology consists of the following steps:

1. Parametrization of geometry and material properties;
2. Definition of the parameter range;
3. Selection of the parameter space sampling algorithm;
4. Selection of the algorithms used to create a surrogate model;
5. Generate a parameter space sampling and run the parametric numerical model;
6. Collect the results and fit/train the different models;
7. Evaluate the surrogate model prognosis qualities;
8. Select the best surrogate model (metamodel of optimal prognosis).

2.3 MOP results

The motor optimization approach was tested in the base speed region of the described machine. The optimization workflow was built in ANSYS optiSLang software. The MOP was calculated after two different sensitivity analyses. In the first attempt, a rough model was created based on 300 design point simulations and using the input parameter reduction approach. The response surface plots of the average torque, MTPA current angle and torque ripple as a function of the most important input parameters are shown in Figs. 6, 7 and 8, respectively.

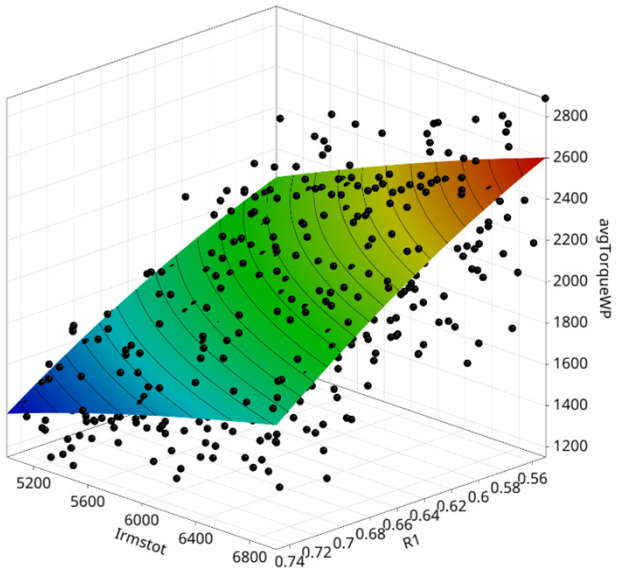

Fig. 6 Response surface plot of average torque in function of the total current and parameter R1

The torque-current angle curves of the design points are shown in Fig. 9. The reference design curve is highlighted in blue color. The CoP matrix of the resulting metamodel is shown in Fig. 10. The total CoP values of the output parameters are marked in red, the most important input parameters for the different output parameters are marked in blue color. The overall (total) quality of the model is satisfactory for testing reasons even with the relatively small number of design points: the lowest value of the total CoP is 73.7% in the case of the current angle output parameter, which is acceptable. The value increased to 82.1% after the second attempt with 600 design points.

The selected metamodel (highest CoP) was the Deep Infinite Mixture Gaussian Processes algorithm (DIM-GP) included in the optiSLang software (developed by PI Probaligence).

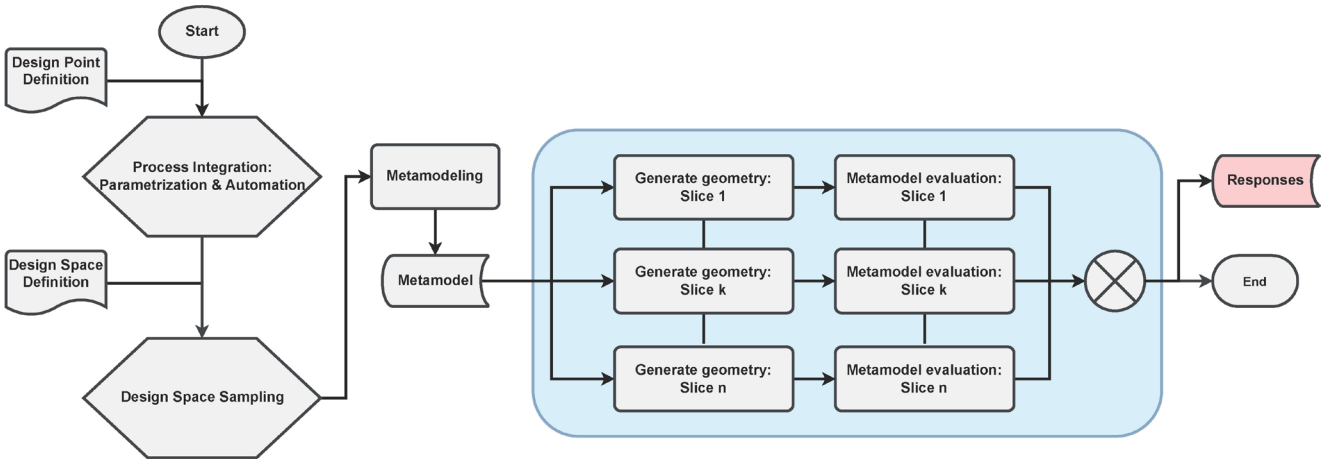

Fig. 5 Single-Surrogate Multi-Slice Method (SS-MSM)

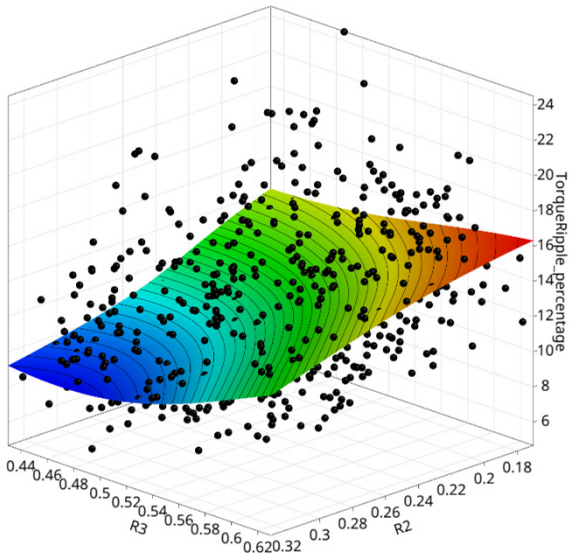

Fig. 7 Response surface plot of the torque ripple in function of R2 and parameter R3

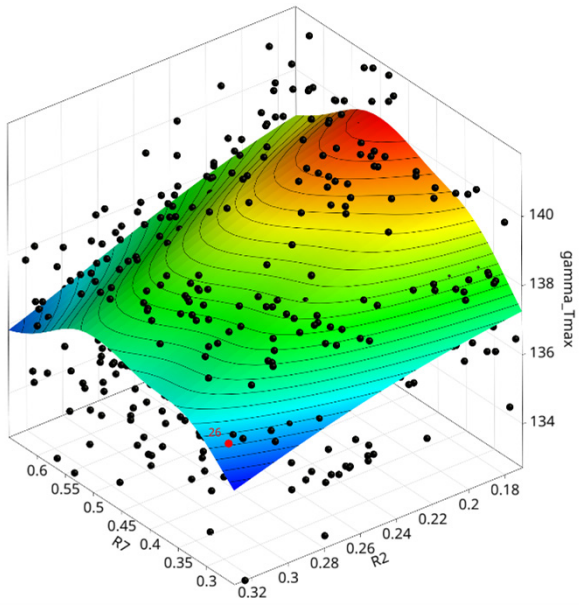

Fig. 8 Response surface plot of the optimum current angle in function of parameters R2 and R7

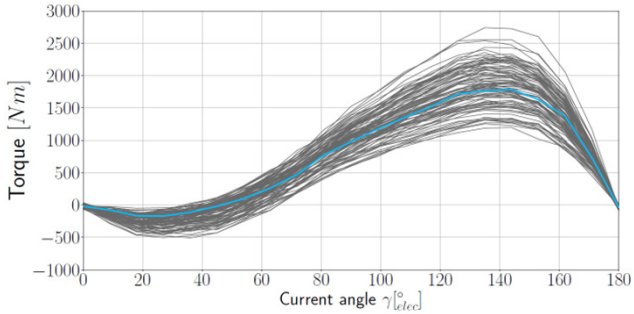

Fig. 9 Torque – current angle curves of the different design points

	l_S	l_R	R_1	R_2	R_3	R_4	R_5	R_6	R_7	$Total$
T_{avg}	1.7	4.5	63.0	8.7	2.7	0.4	6.9	1.3	13.6	99.5
T_{rp}	4.7	1.6	1.1	40.2	31.2	5.0	4.4	4.2	9.2	90.5
γT_{max}	11.0	10.9	0.0	27.9	10.9	8.0	13.3	9.4	25.2	73.7

Fig. 10 CoP matrix

The algorithm works with neural networks and Gaussian processes simultaneously and can predict the mean value and variance of the output parameters (responses), therefore there is no need for hyperparameter tuning. The algorithm can be used for regression analysis. It is suitable for predicting the noise of the data through training a noise parameter which will result in an automatic detection of outliers. The proposed SS-MSM (Fig. 11) is a general method to model and approximate the 3D electromagnetic properties of the axial flux motor through a single surrogate model which is trained in a series of 2D analyses. The method does not have any restrictions on the machine learning model applied. The method was tested with the common ML models, such as deep neural networks, support vector machines or simple polynomial regression models. However, in the recent study, the DIM-GP algorithm was found to perform the best on the example dataset based on the automatic model evaluation described in Section 2.1.

3 Metamodel-based optimization of the AnR-AFPMSM

Based on the created metamodel, a geometry optimization was performed. Obviously, the design space must be a subspace of the input parameter space of the metamodel, otherwise less accurate extrapolation algorithms are required. In this study, the entire parameter space of the metamodel was used in the optimization: the optimization parameter ranges are therefore the same as in the sensitivity study step.

To efficiently model the motor with reasonable accuracy, the previously described SS-MSM approach was applied. The metamodel was created using data from an electromagnetic model parameterized using the ratio-based approach, described in the next section. In this example, an evolutionary algorithm was chosen as the optimization algorithm. Genetic algorithms are usually a good choice for multi-objective optimization problems, especially where there are many input parameters. However, an advantage of the metamodel-based optimization approach is, that the mathematical functions (metamodels) that form the basis of the optimization are smoother functions compared to the original direct data. Therefore, the metamodel can efficiently filter the noise, that otherwise limits the applicable optimization algorithms. In the case of the metamodel-based optimization approach, a wider range of

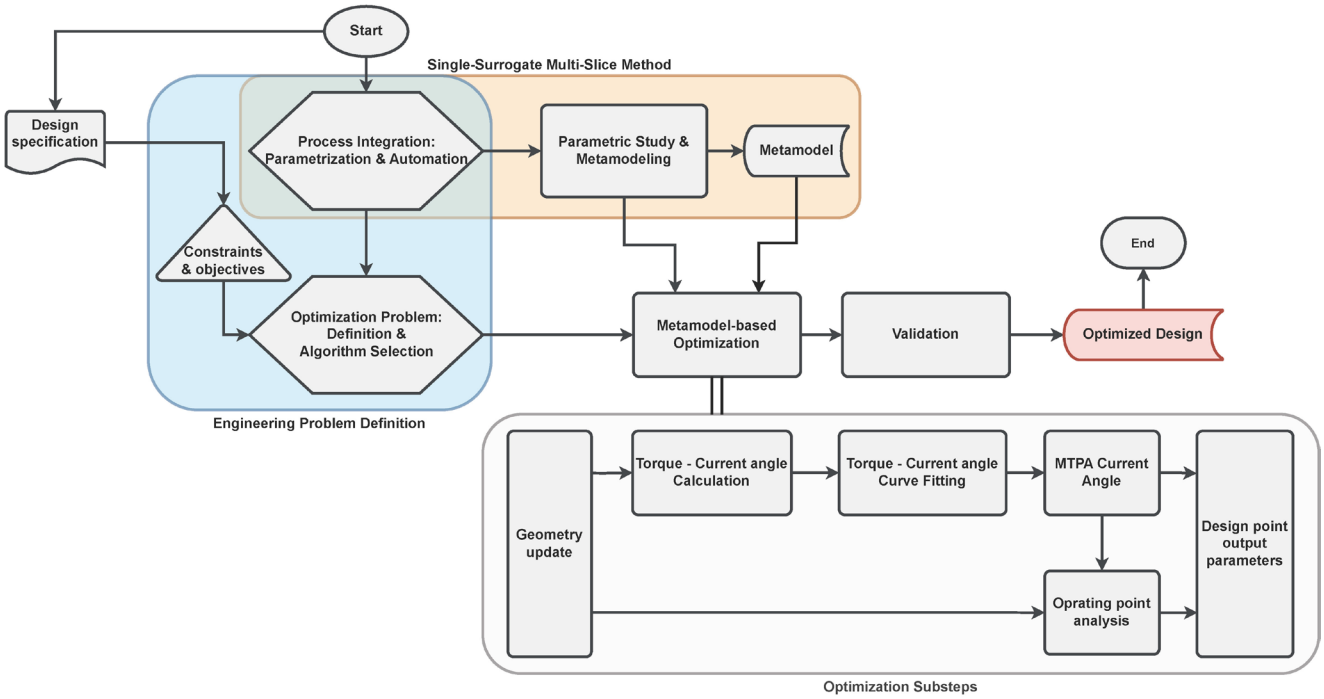

Fig. 11 SS-MSM-based optimization method of the AnR-AFPMSM

optimization algorithms can be selected, also considering the shorter design point evaluation time. Since optimization is performed on a metamodel without direct physics-based simulations, the optimal designs need to be validated by real solver executions (Fig. 11).

3.1 Ratio-based geometry parametrization

To efficiently reduce the number of failed designs during the optimization due to infeasible geometry, the ratio-based parametrization has been implemented. To define the necessary ratio parameters, some parameters must be selected as reference. In this optimization case, the stator outer diameter D_{So}, the stator active length l_S, the rotor active length l_R have been selected. The airgap length l_g is kept as a direct dimensional parameter.

The ratios are formulated by Eqs. (7)–(27). R_1 is the ratio of the stator outer and inner diameters:

$$R_1 = \frac{D_{Si}}{D_{So}}. \tag{7}$$

R_2 is the magnet width ratio in layer 1:

$$R_2 = \frac{w_{pm1}}{\tau_s}. \tag{8}$$

R_2 is the magnet width ratio in layer 2:

$$R_3 = \frac{w_{pm2}}{\tau_p}. \tag{9}$$

R_4 is the magnet length ratio in layer 1:

$$R_4 = \frac{l_{pm1}}{l_R}. \tag{10}$$

R_5 is the magnet length ratio in layer 2:

$$R_5 = \frac{l_{pm2}}{l_R}. \tag{11}$$

R_6 is the ratio controlling the axial position of the permanent magnet in layer 1:

$$R_6 = \frac{d_{pm1} - 0.5l_S - l_g}{l_R}. \tag{12}$$

R_7 is the ratio controlling the radial position of the permanent magnet in layer 2:

$$R_7 = \frac{d_{pm2} - d_{pm1} - l_{pm1}}{0.5l_S + l_g + l_R - d_{pm1} - l_{pm1}}. \tag{13}$$

R_8 is the tooth width ratio:

$$R_8 = \frac{w_t}{\tau_s}. \tag{14}$$

Ratios R_9–R_{12} define the flux barrier geometry according to Eqs. (15)–(18):

$$R_9 = \frac{p1x2 - w_{pm1}}{\tau_p - w_{pm1}}; \tag{15}$$

$$R_{10} = \frac{p1x1 - w_{pm1}}{p1x2 - w_{pm1}}; \tag{16}$$

$$R_{11} = \frac{p1x4 - w_{pm1}}{\tau_p - w_{pm1}}; \tag{17}$$

$$R_{12} = \frac{p1x3 - w_{pm1}}{p1x4 - w_{pm1}}. \tag{18}$$

Ratios R_{13}–R_{16} define the flux barrier geometry according to Eqs. (19)–(22):

$$R_{13} = \frac{p2x2 - w_{pm2}}{\tau_p - w_{pm2}}; \tag{19}$$

$$R_{14} = \frac{p2x1 - w_{pm2}}{p2x2 - w_{pm2}}; \tag{20}$$

$$R_{15} = \frac{p2x4 - w_{pm2}}{\tau_p - w_{pm2}}; \tag{21}$$

$$R_{16} = \frac{p2x3 - w_{pm2}}{p2x4 - w_{pm2}}. \tag{22}$$

Ratios R_{17} and R_{18} define the magnet axial positions in layers 1 and 2 according to Eqs. (23)–(24):

$$R_{17} = \frac{p1y}{d_{pm1} - 0.5l_S - l_g}; \tag{23}$$

$$R_{18} = \frac{p2y}{d_{pm2} - 0.5l_S - l_g}. \tag{24}$$

Ratios R_{19}, R_{20} and R_{21} control the tooth tip (and slot opening) dimensions of the stator according to Eqs. (25)–(27).

$$R_{19} = \frac{w_{tt}}{\tau_s - w_t}. \tag{25}$$

$$R_{20} = \frac{p_{tt1}}{l_S}; \tag{26}$$

$$R_{21} = \frac{p_{tt2} - p_{tt1}}{l_S}. \tag{27}$$

3.2 Optimization problem definition

The input parameter ranges are presented in Table 3, and the motor requirements are summarized in Table 4. The optimization constraints and objectives are a reduced set of motor requirements to keep the optimization problem reasonably simple for this study. Therefore, continuous power requirements are not included, and the thermal model has not been coupled to the simulation model in this case.

Table 3 Geometrical ratios as optimization input parameters of the AnR-AFPMSM

ID	Ref.	Description	Range
D_{So}	400	Stator outer diameter [mm]	400
l_S	60	Stator active length [mm]	50-70
l_R	55	Rotor active length [mm]	45-65
l_g	0.8	Airgap length [mm]	0.80-1.10
R_1	0.6	Diameter ratio, Eq. (6)	0.55-0.75
R_2	0.250	PM width ratio (1), Eq. (7)	0.17-0.33
R_3	0.488	PM width ratio (2), Eq. (8)	0.43-0.63
R_4	0.089	PM length ratio (1), Eq. (9)	0.05-0.13
R_5	0.196	PM length ratio (2), Eq. (10)	0.08-0.22
R_6	0.065	PM location (1), Eq. (11)	0.03-0.11
R_7	0.559	PM location (2), Eq. (12)	0.25-0.65
R_8	0.625	Tooth width ratio, Eq. (13)	0.50-0.65
R_9	0.060	Flux barrier (1) ratio, Eq. (14)	0.02-0.10
R_{10}	0.480	Flux barrier (1) ratio, Eq. (15)	0.38-0.58
R_{11}	0.150	Flux barrier (1) ratio, Eq. (16)	0.10-0.20
R_{12}	0.810	Flux barrier (1) ratio, Eq. (17)	0.71-0.91
R_{13}	0.410	Flux barrier (2) ratio, Eq. (18)	0.31-0.51
R_{14}	0.390	Flux barrier (2) ratio, Eq. (19)	0.30-0.48
R_{15}	0.640	Flux barrier (2) ratio, Eq. (20)	0.54-0.74
R_{16}	0.580	Flux barrier (2) ratio, Eq. (21)	0.48-0.68
R_{17}	0.790	Flux barrier (1) ratio, Eq. (22)	0.69-0.89
R_{18}	0.970	Flux barrier (2) ratio, Eq. (23)	0.95-0.99
R_{19}	0.275	Tooth tip ratio 1, Eq. (24)	0.15-0.40
R_{20}	0.030	Tooth tip ratio 2, Eq. (25)	0.02-0.04
R_{21}	0.030	Tooth tip ratio 3, Eq. (26)	0.02-0.04

Table 4 Optimization problem: constraints and objectives

ID	Type	Formulation	Description
D_{So}	Constraint	$D_{So} < x$	Max. stator outer diameter
D_{Si}	Constraint	$D_{Si} > y$	Min. stator inner diameter
l	Constraint	$(l_S + l_R + l_g) <$ x	Max. active length
I_{Slot}	Constraint	$I_{Slot} < x$	Max. slot current density
T_{RP}	Constraint	$T_{RP} < x$	Max. torque ripple
T_{EM}	Objective	max. T_{EM}	Maximize EM torque

3.3 Optimization method

The geometric optimization of an electric motor with anisotropic (salient) rotor design is a nested optimization

problem. Since the geometry changes during the optimization, the optimal current angle is not constant. Depending on the control method used, the optimal current angle needs to be determined at each step.

Therefore, a large number of iterations are required. In this study, a two-step method is proposed, as shown in Fig. 11. As shown in the figure, the process starts with a simple magnetostatic analysis to determine the static torque-current angle curve for the given geometry. In the proposed method, an approximation curve was fitted to the magnetostatic analysis data at each iteration. The optimum current angle was determined by an optimization algorithm based on the curve and the control algorithm applied.

The optimization algorithm used for geometry optimization is a general-purpose evolutionary algorithm (genetic algorithm, [22]), but other algorithms can also be used. The optimized geometry parameters are shown in Table 5 and illustrated in Fig. 12.

4 Conclusion

The study presents a metamodel-based (surrogate model-based) optimization method for an anisotropic rotor axial flux permanent magnet synchronous motor. The single surrogate multi-slice method was proposed and described in detail. This new method allows for the creation of a single surrogate model and evaluation of multiple parameter-sets based on the number of 2D slices used in the model. This method requires only one training set, but allows for an unlimited number of slices, minimizing the approximation error of the 2D model. In the proposed method, the current angle is optimized according to the MTPA condition in the base-speed region. This method enables reasonably accurate numerical optimization of axial flux motors with complex anisotropic rotor designs using normal computational resources. The optimization example considers a reduced set of electromagnetic design aspects to simplify the problem. However, additional electromagnetic constraints and objectives can be included without major modifications to the workflow. To analyze continuous working performance, an analytical or numerical thermal model must be coupled, which will be described in a later article.

Table 5 Optimized absolute geometric parameters of the AnR-AFPMSM reference design

ID	Reference value	Description
D_{So}	400 mm	Stator outer diameter
D_{Si}	260 mm	Stator inner diameter
l_S	57 mm	Stator active length
l_R	65 mm	Rotor active length
l_g	1.0 mm	Airgap length
w_{pm1}	31.4 mm	Magnet width, layer 1
w_{pm2}	49.5 mm	Magnet width, layer 2
l_{pm1}	6.1 mm	Magnet length, layer 1
l_{pm2}	14.3 mm	Magnet length, layer 2
d_{pm1}	37.6 mm	Magnet position, layer 1
d_{pm2}	71.1 mm	Magnet position, layer 2
w_S	17.25 mm	Slot width
τ_S	43.1 mm	Slot pitch
τ_P	103.7 mm	Pole pitch
p_{1x1}	33.43 mm	Flux barrier, layer 1 (Fig. 2)
p_{1x2}	35.68 mm	Flux barrier, layer 1 (Fig. 2)
p_{1x3}	40.11 mm	Flux barrier, layer 1 (Fig. 2)
p_{1x4}	42.17 mm	Flux barrier, layer 1 (Fig. 2)
p_{2x1}	58.14 mm	Flux barrier, layer 1 (Fig. 2)
p_{2x2}	71.64 mm	Flux barrier, layer 1 (Fig. 2)
p_{2x3}	69.54 mm	Flux barrier, layer 1 (Fig. 2)
p_{2x4}	84.05 mm	Flux barrier, layer 1 (Fig. 2)
p_{1y}	1.54 mm	Flux barrier (Fig. 2)
p_{2y}	26.49 mm	Flux barrier (Fig. 2)

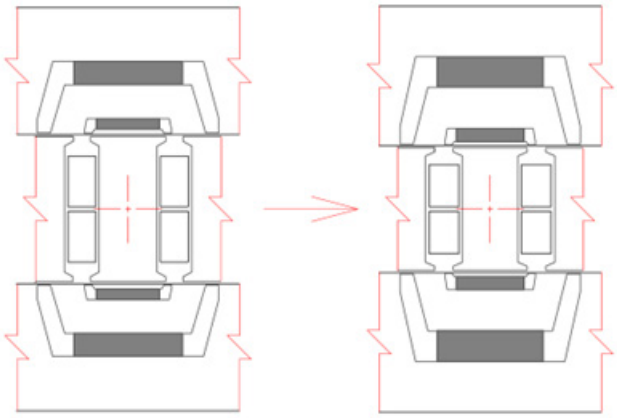

Fig. 12 Original and optimized geometry of the AnR-AFPMSM

References

[1] Vansompel, H., Sergeant, P., Dupré, L. "Optimized Design Considering the Mass Influence of an Axial Flux Permanent-Magnet Synchronous Generator with Concentrated Pole Windings", IEEE Transactions on Magnetics, 46(12), pp. 4101–4107, 2012. https://doi.org/10.1109/TMAG.2010.2070075

[2] Aydin, M., Huang, S., Lipo, T. A. "Optimum design and 3D finite element analysis of non-slotted and slotted internal rotor type axial flux PM disc machines", In: 2001 Power Engineering Society Summer Meeting, Conference Proceedings, Vancouver, Canada, 2001, pp. 1409–1416, 2001. ISBN: 0-7803-7173-9 https://doi.org/10.1109/PESS.2001.970283

[3] Nyitrai, A., Kuczmann, M. "Magnetic equivalent circuit and finite element modelling of anisotropic rotor axial flux permanent magnet synchronous motors with fractional slot distributed winding", IET Electric Power Applications, 17(5), pp. 709–720, 2023. https://doi.org/10.1049/elp2.12298

[4] Vagati, A., Pellegrino, G., Guglielmi, P. "Comparison between SPM and IPM motor drives for EV application", In: The XIX International Conference on Electrical Machines - ICEM 2010, Rome, Italy, 2010, pp. 1–6. ISBN: 978-1-4244-4174-7 https://doi.org/10.1109/ICELMACH.2010.5607911

[5] Tiegna, H., Amara, Y., Barakat, G. "Validity domain of a quasi-3D multislice analytical model for synchronous axial flux machines with trapezoidal magnets", EPJ Applied Physics, 70(1), 10902, 2015. https://doi.org/10.1051/epjap/2015140495

[6] Gulec, M., Aydin, M. "Implementation of different 2D finite element modelling approaches in axial flux permanent magnet disc machines", IET Electric Power Applications, 12(2), pp. 195–202, 2018. https://doi.org/10.1049/iet-epa.2017.0434

[7] Cavagnino, A., Lazzari, M., Profumo, F., Tenconi, A. "A comparison between the axial flux and the radial flux structures for PM synchronous motors", IEEE Transactions on Industry Applications, 38(6), pp. 1517–1524, 2002. https://doi.org/10.1109/TIA.2002.805572

[8] Riba, J. R., López-Torres, C., Romeral, L., Garcia, A. "Rare-earth-free propulsion motors for electric vehicles: A technology review", Renewable and Sustainable Energy Reviews, 57, pp. 367–379, 2016. https://doi.org/10.1016/j.rser.2015.12.121

[9] Paar, C., Muetze, A. "Quantification of External Heat Load on HEV Integrated IPMs Using the Air-Gap Shear Stress", IEEE Transactions on Industry Applications, 53(3), pp. 1909–1919, 2017. https://doi.org/10.1109/TIA.2017.2656069

[10] Krasopoulos, C. T., Beniakar, M. E., Kladas, A. G. "Multicriteria PM Motor Design Based on ANFIS evaluation of EV Driving Cycle Efficiency", IEEE Transactions on Transportation Electrification, 4(2), pp. 525–535, 2018. https://doi.org/10.1109/TTE.2018.2810707

[11] Benlamine, R., Dubas, F., Randi, S. A., Lhotellier, D., Espanet, C. "Modeling of an axial-flux interior PMs machine for an automotive application using magnetic equivalent circuit", In: 2015 18th International Conference on Electrical Machines and Systems (ICEMS), Pattaya City, Thailand, 2015, pp. 1266–1271. ISBN: 978-1-4799-8804-4 https://doi.org/10.1109/ICEMS.2015.7385234

[12] Chen, Q., Liang, D., Liu, Y., Wang, Q. "Design and multi-object optimisation of axial flux interior PMSM for EV and HEV applications", The Journal of Engineering, 2017(13), pp. 2215–2220, 2017. https://doi.org/10.1049/joe.2017.0724

[13] Nyitrai, A., Szabó, G., Horváth, S. R. "Parameter Determination and Drive Control Analysis of Axial Flux Permanent Magnet Synchronous Motors", Periodica Polytechnica Electrical Engineering and Computer Science, 66(2), pp. 205–214, 2022. https://doi.org/10.3311/PPee.19714

[14] Lim, D. K., Woo, D. K., Kim, I. W., Ro, J. S., Jung, H. K. "Cogging Torque Minimization of a Dual-Type Axial-Flux Permanent Magnet Motor Using a Novel Optimization Algorithm", IEEE Transactions on Magnetics, 49(9), pp. 5106–5111, 2013. https://doi.org/10.1109/TMAG.2013.2256430

[15] You, Y. M. "Multi-objective optimization of a permanent magnet synchronous motor based on an automated design and analysis procedure", Microsystem Technologies, 26(11), pp. 3477–3488, 2020. https://doi.org/10.1007/s00542-020-04929-z

[16] Riviere, N., Villani, M., Popescu, M. "Optimisation of a High Speed Copper Rotor Induction Motor for a Traction Application", In: Proceedings. IECON 2019 – 45th Annual Conference of the IEEE Industrial Electronics Conference, Lisbon, Portugal, 2019, pp. 2720–2725. ISBN: 978-1-7281-4878-6 https://doi.org/10.1109/IECON.2019.8927627

[17] Tang, N., Sossong, D., Krause, N., Hou, X., Liben, M. J. T., Ludois, D. C., Brown, I. P. "Implementation of a Metamodel-Based Optimization for the Design of a High Power Density Wound Field Traction Motor", IEEE Transactions on Industry Applications, 59(6), pp. 6726–6735, 2023. https://doi.org/10.1109/TIA.2023.3309616

[18] Jang, G. U., Kim, C. W., Bae, D., Cho, Y., Lee, J. J., Cho, S. "Reliability-based robust design optimization for torque ripple reduction considering manufacturing uncertainty of interior permanent magnet synchronous motor", Journal of Mechanical Science and Technology, 34(3), pp. 1249–1256, 2020. https://doi.org/10.1007/s12206-020-0223-3

[19] Will, J., Most, T. "Metamodell of optimized Prognosis (MoP) - an Automatic Approach for User Friendly Parameter Optimization Metamodel approaches Polynomial least square approximation", In: ANSYS Conference & 27. CADFEM Users' Meeting 2009. Conference proceedings, Leipzig, Germany, 2009, pp. 1–18. https://doi.org/10.13140/2.1.4946.9122

[20] Wisnowski, J. W., Simpson, J. R., Montgomery, D. C., Runger, G. C. "Resampling methods for variable selection in robust regression", Computational Statistics & Data Analysis, 43(3), pp. 341–355, 2003. https://doi.org/10.1016/S0167-9473(02)00235-9

[21] Bucher, C. "Basic concepts for robustness evaluation using stochastic analysis", In: Efficient Methods for Robust Design and Optimization – EUROMECH Colloquium 482, London, UK, 2007.

[22] Deb, K., Pratap, A., Agarwal, S., Meyarivan, T. "A fast and elitist multiobjective genetic algorithm: NSGA-II", IEEE Transactions on Evolutionary Computation, 6(2), pp. 182–197, 2002. https://doi.org/10.1109/4235.996017